Published in final edited form as:
J Biol Inorg Chem. 2010 January ; 15(1): 99–105. doi:10.1007/s00775-009-0598-1.

Copper Redistribution in Atox1-deficient Mouse Fibroblast Cells

Reagan McRae, **Barry Lai**, and **Christoph J. Fahrni**
Reagan McRae · Christoph J. Fahrni, School of Chemistry and Biochemistry, Petit Institute for Bioengineering and Bioscience, Georgia Institute of Technology, 901 Atlantic Drive, Atlanta, Georgia 30332, U.S.A, fahrni@chemistry.gatech.edu

Barry Lai, X-ray Science Division, Advanced Photon Source, Argonne National Laboratory, Argonne, IL 60439

Abstract

Quantitative SXRF imaging of adherent mouse fibroblast cells deficient in Atox1, a metallochaperone protein responsible for delivering copper (Cu) to cuproenzymes in the trans-Golgi network, revealed striking differences in the subcellular Cu distribution compared to wildtype cells. While the latter showed a pronounced perinculear localization of Cu, the Atox1-deficient cells displayed a mostly unstructured and diffuse distribution throughout the entire cell body. Comparison of the SXRF elemental maps for Zn and Fe of the same samples showed no marked differences between the two cell lines. The data underscore the importance of Atox1, not only as a metallochaperone for delivering Cu to cuproenzymes, but also as a key player in maintaining the proper distribution and organization of Cu at the cellular level.

Keywords

Synchrotron X-ray fluorescence; Elemental imaging; Menkes disease; Golgi apparatus

Introduction

Copper (Cu) is a trace metal essential for the maintenance of human health. Serving as a cofactor for a number of enzymes, Cu plays an important role in a broad range of biological processes including cellular respiration, free radical defense, iron mobilization and uptake, formation of connective tissue, pigmentation, blood clotting, and the synthesis of neurotransmitters [1]. Conversely, cellular Cu accumulation to excessive levels is detrimental as it catalyzes the formation of reactive oxygen species (ROS) that may damage DNA, proteins, and other biomolecules, thus resulting in increased oxidative stress and ultimately cell death [2,3]. Given this dualistic nature, cells have evolved an intricate machinery for transport, storage and regulation of intracellular Cu, such that sufficient amounts are available to fulfill its essential roles while avoiding accumulation to potentially damaging levels [4–9]. Instances of Cu imbalance or homeostatic dysfunction have been directly associated with a number of neurological diseases, including Menkes disease [10,11], Wilson's disease [12–14], Alzheimer's disease [15–19], Parkinson's disease [16–18], and amyotrophic lateral sclerosis [17,20,21], further highlighting the necessity for tightly controlled levels of intracellular Cu [22–24].

The discovery of genes coding for proteins involved in Cu-uptake, transport and regulation led to the identification of a host of proteins involved in Cu homeostasis. On a cellular level,

Correspondence to: Christoph J. Fahrni.

Cu is imported across the plasma membrane via the high affinity Cu transporter Ctr1, and subsequently partitioned into distinct trafficking pathways that involve specialized metallochaperones [25–29]. For example, the Cu chaperone Ccs is responsible to escort and incorporate Cu into cytoplasmic superoxide dismutase (SOD) [30,31]. Likewise, the three chaperone proteins Cox17, Cox11, and Sco1 deliver Cu to mitochondrial cytochrome c oxidase [32–35], and the copper chaperone Atox1 is critical for transport of Cu to either the Menkes (ATP7a) or Wilson's (ATP7b) disease ATPases situated in the trans-Golgi network (TGN) [36–38], where it is delivered either to cuproenzymes such as ceruloplasmin and lysyl oxidase, or trafficked through the secretory pathway for extracellular release [39].

While significant progress has been made towards the mechanistic understanding of cellular Cu homeostasis at the molecular level, important questions remain regarding the maintenance of Cu at the cellular level. For example, Cu uptake and release occur with a surprisingly rapid kinetics [40], suggesting that a portion of the total cellular Cu is present in a kinetically labile form and thus readily available for distribution and uptake into cuproenzymes; however, the nature of this labile pool, its subcellular localization, and potential alterations in diseases associated with defects in Cu trafficking are poorly understood. In view of the potential toxicity of Cu, a detailed understanding of the redistribution and mislocalization of labile Cu in these diseases is of particular importance.

Several cell lines have been created that may serve as model systems to investigate the potential Cu redistribution associated with defects in Cu trafficking pathways. In this report, we focused on studying the subcellular Cu distribution in $Atox1^{-/-}$ fibroblasts, an embryonic mouse cell line that is deficient in the chaperone protein Atox1 responsible for trafficking of Cu to the TGN network [36]. The protein Atox1 was originally discovered through its yeast homologue Atx1, which showed a protective function against superoxide and peroxide toxicity [41]. The $Atox1^{-/-}$ cell line was created by disruption of the Atox1 locus through gene-trap insertion of a β-galactosidase-neomycin marker in mouse embryonic stem cells [37]. Mice deficient for Atox1 display a severe phenotype characterized by growth retardation, perinatal mortality, and congenital malformations, much like the phenotype observed in Menkes' disease [37]. At the cellular level, significant differences in the Cu-mediated trafficking of the Menkes ATPase from the TGN to cytosolic vesicular compartments were observed between $Atox1^{+/+}$ and $Atox1^{-/-}$ cells [36]. While $Atox1^{-/-}$ cells still showed a Cu-dependent translocation of the Menkes protein out of the TGN compartments, the movement was significantly impaired in a dose and time-dependent manner. Most recently, Atox1 has been also implied as a Cu-dependent transcription factor that mediates Cu-induced cell proliferation [42]. In view of the essential role of Atox1 in cellular Cu trafficking and homeostasis, the elucidation of differences in the subcellular Cu distribution between $Atox1^{+/+}$ and $Atox1^{-/-}$ cells was of particular interest.

To quantify the distribution of Cu at the subcellular level, highly sensitive microanalytical techniques are required. While the sensitivity of traditional methods, such as inductively coupled plasma mass spectrometry (ICP-MS), atomic emission spectroscopy, (AE) or x-ray fluorescence analysis (XRF) is insufficient for analyzing the elemental contents of a single cell, several more recently developed techniques, notably secondary ion mass spectrometry (SIMS), nuclear microprobes (PIXE or PIGE), and synchrotron x-ray fluorescence microscopy (SXRF, SRIXE, or microXRF) offer sufficient sensitivity to obtain spatially resolved elemental maps at the subcellular level [43–47]. These new imaging techniques have already provided important insights into the localization of Cu pools within individual cells. For example, an SXRF study of Cu-loaded NIH 3T3 cells yielded detailed topographical elemental maps and suggested the presence of a labile Cu pool in the TGN region and mitochondria [48]. High-resolution SXRF imaging of human microvascular endothelial cells revealed an intriguing relocalization of Cu from intracellular compartments

towards the tips of filopodia, thus highlighting the importance of endogenous Cu during angiogenesis [49]. A similar Cu accumulation was recently described in thin neurites formed upon nerve growth factor (NGF) stimulated differentiation of rat pheochromocytoma (PC12) cells, which were used as an in vitro model of dopaminergic cells [50]. Given these early successes in imaging the subcellular distribution of Cu with great detail, SXRF imaging seemed ideally poised for studying the effects of Cu relocalization in cells with altered trafficking pathways.

Materials and Methods

Reagents and Materials

The wildtype Atox1$^{+/+}$ and Atox1$^{-/-}$ embryonic mouse fibroblast cell lines were a generous gift from Jonathan D. Gitlin [36]. The cells were cultured in Dulbecco's modified Eagle's medium (DMEM, GIBCO-BRL, Gaithersburg, USA) supplemented with 10% bovine serum (GIBCO), 200 mM L-glutamine (GIBCO), 250 μg/mL geneticin (GIBCO), penicillin (100 IU/mL) and streptomycin (100 mg/L) at 37°C under an atmosphere of humidified air containing 5% CO_2. The culture medium was sterilized by filtration through 0.2 μm filters.

Sample Preparation

Cells were grown to 50–80% confluency on silicon nitride windows (2 × 2 × 0.0005 mm, Silson Ltd., UK) that were pre-treated for 30 min with 0.01% poly-L-lysine solution (Sigma-Aldrich). For preparations in basal medium, cells were directly seeded in 6-well culture plates containing the silicon to reach the desired confluency. For experiments that nitride windows and grown at 37°C/5% CO_2 involved supplementation of the culture medium with Cu(II), cells were first grown in basal medium to 50% confluency as described above, then switched for 24 h to basal medium containing 200 μM bathocuproine disulphonate (BCS, Sigma-Aldrich), thoroughly washed with 1X-PBS (pH 7.2, pre-warmed to 37°C), and finally incubated in full growth media supplemented with 50 μM $CuCl_2$ (Sigma-Aldrich) for 4 h at 37°C.

Following the growth/incubation conditions described above, cells were further prepared for SXRF experiments as previously described [51]. Briefly, cells were washed with PBS (pre-warmed at 37°C), and fixed for 10 min at room temperature with 3.7% paraformaldehyde (Sigma-Aldrich, freshly prepared solution in PBS). After thoroughly washing with PBS, the samples were rinsed twice with sterile dH_2O followed by two brief washes with isotonic ammonium acetate (Sigma-Aldrich, 0.1 M solution in sterile dH_2O). Finally, samples were air-dried overnight in a covered sterile cell culture dish.

Synchrotron Radiation X-ray Fluorescence Microscopy (SXRF)

Synchrotron radiation x-ray fluorescence (SXRF) microscopy was performed at the 2-ID-D beamline of the Advanced Photon Source located at Argonne National Laboratory (IL, USA). The air-dried cells grown on silicon nitride windows were placed onto a kinematic specimen holder suitable for both optical and x-ray fluorescence microscopy. The holder was mounted on a light microscope (Leica DMXRE) and target cells were located on the grid relative to a pre-determined reference point using a motorized x/y stage (Ludl Bioprecision). Coordinates were recorded and used to precisely locate the target cell(s) once the grid was transferred to the microprobe. For XRF excitation, a monochromatic X-ray beam generated by an undulator source was focused to a spot size of 0.5×0.5 μm^2 on the specimen by using a Fresnel zone plate. An excitation energy of 10 keV was chosen to ensure excitation of all first row transition elements as well as Ca and K, although to a lesser extent. The sample was subsequently raster scanned through the beam at 298K under a helium atmosphere. The pixel step size was set to 0.5 μm and the entire X-ray spectrum was

recorded for each pixel using an energy dispersive germanium detector (Canberra LEGe detector).

Data Analysis

Elemental maps were created by spectral filtering, using spectral regions of interest matched to characteristic x-ray emission lines to determine the fluorescence signal for each element. Calibration to elemental area densities ($\mu g/cm^2$) was done by comparison of x-ray fluorescence signal strength from the sample to fluorescence from thin film standards NBS-1832 and NBS-1833 from the National Bureau of Standards (NBS/NIST, Gaithersburg, MD) using MAPS software [52]. The elemental content was calculated by fitting of individual spectra of the acquired fluorescence datasets, and comparing fitted fluorescence signal strength with that resulting from fitting of NBS 1832/33 standard spectra.

Results and Discussion

To choose growth conditions that would maximize the differences in Cu distribution and thus best reveal the impact of altered Cu trafficking pathways, we utilized earlier studies on the Cu-dependent relocalization of the Menkes ATPase as guidelines [36]. Specifically, the following findings were taken into consideration: (1) the Menkes protein localization and total cellular Cu were identical for both Atox1$^{-/-}$ and wildtype cells under Cu-limiting conditions, where cells were grown in low-serum media supplemented with 200 μM BCS as extracellular Cu(I)-chelator, (2) differences in Cu-mediated trafficking out of the TGN were most pronounced when the medium was supplemented with 10 μM $CuCl_2$ following BCS treatment, and (3) the impaired Menkes protein trafficking in Atox1$^{-/-}$ cells could be rescued by supplementation with ≥ 100 μM $CuCl_2$ and extended incubation periods (> 4 h) [36]. Based on these data we anticipated that differences in Cu distribution between Atox1$^{-/-}$ and wildtype cells would be most pronounced when cells were pretreated with 200 μM BCS for 48 hours followed by supplementation with 10 but less than 100 μM $CuCl_2$ in full media over a period of 4 hours. Although no data were provided for the intermediated concentration range, supplementation with 50 μM $CuCl_2$ appeared to strike the best balance between improving the signal-to-noise ratio for SXRF detection while still maintaining the delayed Menkes trafficking in Atox1$^{-/-}$ cells. As a control, both cells lines were also cultured under basal conditions in full media without supplementation. Adherent cells were directly grown on a x-ray compatible substrate (silicon nitride), chemically fixed, and dried in air. Individual cells were raster scanned with excitation at 10.0 keV with 0.5 μm step size, yielding 2D maps for all biologically relevant first row transition elements. The considerable size of adherent fibroblast cells combined with the necessity to obtain elemental maps with high spatial resolution resulted in long data acquisition times (2–4 hours per cell), and therefore restricted the sample size to only three repeats for each growth condition and cell type. Quantitative elemental maps for Cu, Zn, and Fe were analyzed in terms of the total cellular content as well as the nuclear and cytoplasmic portions (Table 1). To account for differences in cell size that might also contribute to differences in trace metal content, the data are listed as densities in units of $pmol/cm^2$. For ease of comparison, the density data compiled in Table 1 are also illustrated in a set of three bar graphs (Figure 1).

Basal Growth Conditions

Due to the low cellular Cu content under these growth conditions, the signal-to-noise ratios of the resulting SXRF maps were insufficient to accurately assess differences in the subcellular Cu distribution between the two cell lines. Nevertheless, integration of the Cu signal in the nucleus compared to cytoplasm revealed significant differences between Atox1$^{-/-}$ and wildtype control cells (Table 1). Consistent with previous findings based on

atomic absorption spectroscopy of bulk samples [36], Atox1$^{-/-}$ cells significantly accumulated Cu due to impaired Cu efflux under these conditions. Furthermore, a recent study with a metallothionein (MT)-knockout cell line showed also increased intracellular Cu levels upon siRNA-mediated knockdown of Atox1 [53]. In wildtype cells, approximately 23% of the total cellular Cu was localized in the nuclear region (Table 1). Interestingly, Atox1$^{-/-}$ cells consistently showed an elevated nuclear Cu content compared to wildtype. In contrast, no significant changes were observed for the Zn and Fe content, neither in the whole cell analysis nor the nuclear/cytoplasmic distribution ratios (Table 1 and Figure 1).

Effect of Cu(II) Supplementation

Wildtype cells incubated with 50 μM $CuCl_2$ for 4 hours displayed a marked increase of the cellular Cu content (Table 1). Interestingly, Atox1$^{-/-}$ cells treated under the same conditions revealed a similar increase of intracellular Cu (Table 1) [36], thus contrasting the observations under basal growth conditions. Nevertheless, these findings are in agreement with the data on bulk samples reported in the literature [36]. While the impaired Cu efflux mechanism in Atox1$^{-/-}$ cells eventually leads to a substantial increase in the intracellular Cu content [37], at early time points the response to elevated extracellular Cu(II) is indistinguishable compared to wildtype cells. Likewise, the ratio of nuclear to total Cu was identical within experimental error for both cell lines and similar to wildtype cells grown under basal conditions. A comparison of the Fe content showed no apparent differences between the two cells lines in response to Cu(II) supplementation, although the ratio of nuclear Fe appeared to be reduced in both cases. Similarly, analysis of the Zn content and relative distribution between nucleus and cytoplasm showed no significant differences and appears to be independent of the cell type and growth conditions with Cu(II) supplementation.

Despite the similarities of the total Cu content, the subcellular distribution, as revealed by the quantitative SXRF maps shown in Figure 2, showed striking differences between Atox1$^{-/-}$ and Atox1$^{+/+}$ cells. The wildtype cell line consistently displayed a strong Cu localization in the perinuclear region with a slightly less pronounced abundance throughout the cytoplasm and within the cell nucleus (Figure 2, top row). Conversely, the Cu distribution in Atox1$^{-/-}$ cells revealed no obvious compartmentalization or subcellular accumulation, but rather a diffuse distribution throughout the entire cell body (Figure 2, bottom row). While both cell lines showed a similar ratio of nuclear to total cellular Cu, the distribution in Atox1$^{-/-}$ cells appeared entirely unstructured and lacked areas of localization as observed in the nucleus of wildtype cells. A comparison with the Zn elemental maps obtained from the same set of cells showed no marked differences between Atox1$^{-/-}$ and wildtype cells (Figure 3).

Previous studies demonstrated that supplementation with 100 μM $CuCl_2$ over a time period of 4 hours resulted in almost complete relocalization of the Menkes ATPase out of the TGN to cytoplasmic compartments [36]. Given the comparable incubation conditions and time course of our SXRF experiments, we can assume that a similar relocalization of the Menkes protein occurred; however, a significant fraction of Cu remained localized in the perinuclear region (Figure 2, top row). While the Cu- dependent trafficking of the Menkes protein out of the TGN is well established [36,54], it still remains to be determined what fraction of cellular Cu is actually relocalized in this process. The SXRF data imply that Cu trafficking and distribution is not exclusively linked with Menkes trafficking at early time points following stimulation with elevated extracellular Cu(II). Taking into account that the requirement for Atox1 in Cu-mediated trafficking of the Menkes protein can be bypassed with excess Cu [36], we cannot exclude the possibility that the diffuse Cu distribution in Atox1$^{-/-}$ cells is a consequence of Cu delivery to Menkes protein containing compartments, either through Atox1-independent loading prior to or after trafficking out of the TGN. Such

a scenario would imply, however, that alternative Atox1-dependent trafficking pathways exist that lead to compartmentalization of Cu in the perinuclear region of the wildtype cells. Alternatively, the diffuse Cu distribution pattern in Atox1$^{-/-}$ cells might be the result of a random redistribution process due to the absence of the regular trafficking pathway.

Conclusions

Spatially well resolved SXRF elemental maps of individual adherent mouse fibroblast cells revealed intriguing differences in the Cu distribution of Atox1$^{-/-}$ cells compared to the corresponding wildtype. While the latter cells showed a distinct perinuclear Cu localization, the distribution in Atox1$^{-/-}$ cells was reproducibly unstructured and diffuse throughout the entire cell. Although the SXRF elemental maps cannot reveal the nature of the associated cellular structure or organelles in absence of a xenobiotic label, the characteristic perinuclear Cu distribution pattern might point towards the involvement of the Golgi apparatus, late endosomes or mitochondria, all of which are typically found in the vicinity of the nuclear envelope. The data highlight the importance of Atox1, not only as a metallochaperone for delivering Cu to cuproenzymes, but as a key player in maintaining the proper distribution and organization of Cu at the cellular level.

Acknowledgments

We thank Jonathan Gitlin (Washington University, St. Louis, USA) for providing us with samples of the Atox1$^{-/-}$ and Atox1$^{+/+}$ cell lines. We also thank Stefan Vogt (Argonne National Laboratory) for providing support with the MAPS software. Financial support from the National Institutes of Health (R01GM067169) is gratefully acknowledged. Use of the Advanced Photon Source was supported by the U.S. Department of Energy, Office of Science, Office of Basic Energy Sciences, under Contract No. DE-AC02-06CH11357.

Abbreviations

Atox1	Antioxidant-1 protein (cytosolic metallochaperone)
BCS	Bathocuproin disulfonate
PBS	Phosphate-buffered saline
SXRF	Synchrotron X-ray fluorescence microscopy
TGN	*trans*-Golgi network
XRF	X-ray fluorescence

References

1. Massaro, EJ., editor. Handbook of Copper Pharmacology and Toxicology. Humana Press; 2002.
2. Stohs SJ, Bagchi D. Free Radic Biol Med. 1995; 18:321–336. [PubMed: 7744317]
3. Valko M, Morris H, Cronin MTD. Curr Med Chem. 2005; 12:1161–1208. [PubMed: 15892631]
4. Harris ED. Ann Rev Nutr. 2000; 20:291–310. [PubMed: 10940336]
5. Puig S, Thiele DJ. Curr Opin Chem Biol. 2002; 6:171–180. [PubMed: 12039001]
6. Kim B-E, Nevitt T, Thiele DJ. Nat Chem Biol. 2008; 4:176–185. [PubMed: 18277979]
7. Bertinato J, L'Abbé MR. J Nutr Biochem. 2004; 15:316–322. [PubMed: 15157936]
8. Lalioti V, Muruais G, Tsuchiya Y, Pulido D, Sandoval IV. Front Biosci. 2009; 14:4878–4903. [PubMed: 19482593]
9. Turski ML, Thiele DJ. J Biol Chem. 2009; 284:717–721. [PubMed: 18757361]
10. Andrews NC. Curr Opin Chem Biol. 2002; 6:181–186. [PubMed: 12039002]
11. de Bie P, Muller P, Wijmenga C, Klomp LWJ. J Med Genet. 2007; 44:673–688. [PubMed: 17717039]

12. Loudianos G, Gitlin JD. Semin Liver Disease. 2000; 20:353–364.
13. Gitlin JD. Gastroent. 2003; 125:1868–1877.
14. Kitzberger R, Madl C, Ferenci P. Metab Brain Dis. 2005; 20:295–302. [PubMed: 16382340]
15. Bush AI. Trends Neurosci. 2003; 26:207–214. [PubMed: 12689772]
16. Bush AI. Curr Opin Chem Biol. 2000; 4:184–191. [PubMed: 10742195]
17. Gaggelli E, Kozlowski H, Valensin D, Valensin G. Chem Rev. 2006; 106:1995–2044. [PubMed: 16771441]
18. Barnham KJ, Bush AI. Curr Opin Chem Biol. 2008; 12:222–228. [PubMed: 18342639]
19. Macreadie IG. Eur Biophys J Biophys Lett. 2008; 37:295–300.
20. Carrí MT, Ferri A, Cozzolino M, Calabrese L, Rotilio G. Brain Res Bull. 2003; 61:365–374. [PubMed: 12909279]
21. Wijesekera LC, Leigh PN. Orphanet J Rare Dis. 2009; 4:3. [PubMed: 19192301]
22. Rae TD, Schmidt PJ, Pufahl RA, Culotta VC, O'Halloran TV. Science. 1999; 284:805–808. [PubMed: 10221913]
23. Finney LA, O'Halloran TV. Science. 2003; 300:931–936. [PubMed: 12738850]
24. Waldron KJ, Rutherford JC, Ford D, Robinson NJ. Nature. 2009; 460:823–830. [PubMed: 19675642]
25. Elam JS, Thomas ST, Holloway SP, Taylor AB, Hart PJ. Advances in Protein Chemistry. 2002:151–219. [PubMed: 12418178]
26. Rosenzweig AC. Acc Chem Res. 2001; 34:119–128. [PubMed: 11263870]
27. Huffman DL, O'Halloran TV. Ann Rev Biochem. 2001; 70:677–701. [PubMed: 11395420]
28. O'Halloran TV, Culotta VC. J Biol Chem. 2000; 275:25057–25060. [PubMed: 10816601]
29. Luk E, Jensen LT, Culotta VC. J Biol Inorg Chem. 2003; 8:803–809. [PubMed: 14517615]
30. Culotta VC, Yang M, O'Halloran TV. Biochim Biophys Acta-Mol Cell Res. 2006; 1763:747–758.
31. Rothstein JD, Becker M, Hoberg MD, Culotta V, Corson L, Cleveland D, Price D, Wong P. Ann Neurol. 1998; 44:7. [PubMed: 9667587]
32. Abajian C, Yatsunyk LA, Ramirez BE, Rosenzweig AC. J Biol Chem. 2004; 279:53584–53592. [PubMed: 15465825]
33. Glerum DM, Shtanko A, Tzagoloff A. J Biol Chem. 1996; 271:14504–14509. [PubMed: 8662933]
34. Pierrel F, Cobine PA, Winge DR. Biometals. 2007; 20:675–682. [PubMed: 17225062]
35. Horng Y-C, Cobine PA, Maxfield AB, Carr HS, Winge DR. J Biol Chem. 2004; 279:35334–35340. [PubMed: 15199057]
36. Hamza I, Prohaska J, Gitlin JD. Proc Natl Acad Sci USA. 2003; 100:1215–1220. [PubMed: 12538877]
37. Hamza I, Faisst A, Prohaska J, Chen J, Gruss P, Gitlin JD. Proc Natl Acad Sci USA. 2001; 98:6848–6852. [PubMed: 11391006]
38. Pufahl RA, Singer CP, Peariso KL, Lin SJ, Schmidt PJ, Fahrni CJ, Culotta VC, Penner-Hahn JE, O'Halloran TV. Science. 1997; 278:853–856. [PubMed: 9346482]
39. Petris MJ, Mercer JFB, Culvenor JG, Lockhart P, Gleeson PA, Camakaris J. EMBO Journal. 1996; 15:6084–6095. [PubMed: 8947031]
40. Herd SM, Camakaris J, Christofferson R, Wookey P, Danks DM. Biochem J. 1987; 247:341–347. [PubMed: 3426541]
41. Lin SJ, Culotta VC. Proc Natl Acad Sci USA. 1995; 92:3784–3788. [PubMed: 7731983]
42. Itoh S, Kim HW, Nakagawa O, Ozumi K, Lessner SM, Aoki H, Akram K, McKinney RD, Ushio-Fukai M, Fukai T. J Biol Chem. 2008; 283:9157–9167. [PubMed: 18245776]
43. McRae R, Bagchi P, Sumalekshmy S, Fahrni CJ. Chem Rev. 2009; 109:4780–4827. [PubMed: 19772288]
44. Fahrni CJ. Curr Opin Chem Biol. 2007; 11:121–127. [PubMed: 17353139]
45. Lobinski R, Moulin C, Ortega R. Biochimie. 2006; 88:1591–1604. [PubMed: 17064836]
46. Ortega R, Devès G, Carmona A. J R Soc Interface. 2009; 6:S649–S658. [PubMed: 19605403]

47. Paunesku T, Vogt S, Maser J, Lai B, Woloschak G. J Cell Biochem. 2006; 99:1489–1502. [PubMed: 17006954]
48. Yang L, McRae R, Henary MM, Patel R, Lai B, Vogt S, Fahrni CJ. Proc Natl Acad Sci USA. 2005; 102:11179–11184. [PubMed: 16061820]
49. Finney L, Mandava S, Ursos L, Zhang W, Rodi D, Vogt S, Legnini D, Maser J, Ikpatt F, Olopade OI, Glesne D. Proc Natl Acad Sci USA. 2007; 104:2247–2252. [PubMed: 17283338]
50. Carmona A, Cloetens P, Devès G, Bohic S, Ortega R. J Anal At Spectrom. 2008; 23:1083–1088.
51. McRae R, Lai B, Vogt S, Fahrni CJ. J Struct Biol. 2006; 155:22–29. [PubMed: 16473527]
52. Vogt S. J Phys IV. 2003; 104:635–638.
53. Miyayama T, Suzuki KT, Ogra Y. Toxicol Appl Pharmacol. 2009; 237:205–213. [PubMed: 19362104]
54. La Fontaine S, Mercer JFB. Arch Biochem Biophys. 2007; 463:149–167. [PubMed: 17531189]

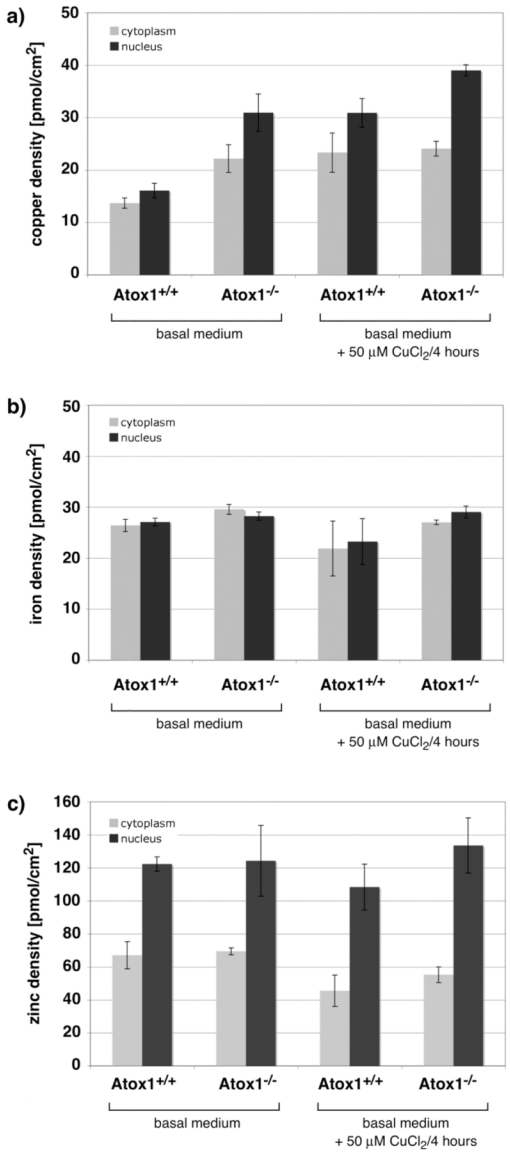

Figure 1.

Trace metal contents of $Atox1^{+/+}$ and $Atox1^{-/-}$ cells cultured in basal medium and medium supplemented with 50 μM $CuCl_2$ for 4 h. The SXRF data were quantitatively analyzed for the content of Cu (a), Fe (b) and Zn (c). The corresponding numerical values are compiled in Table 1.

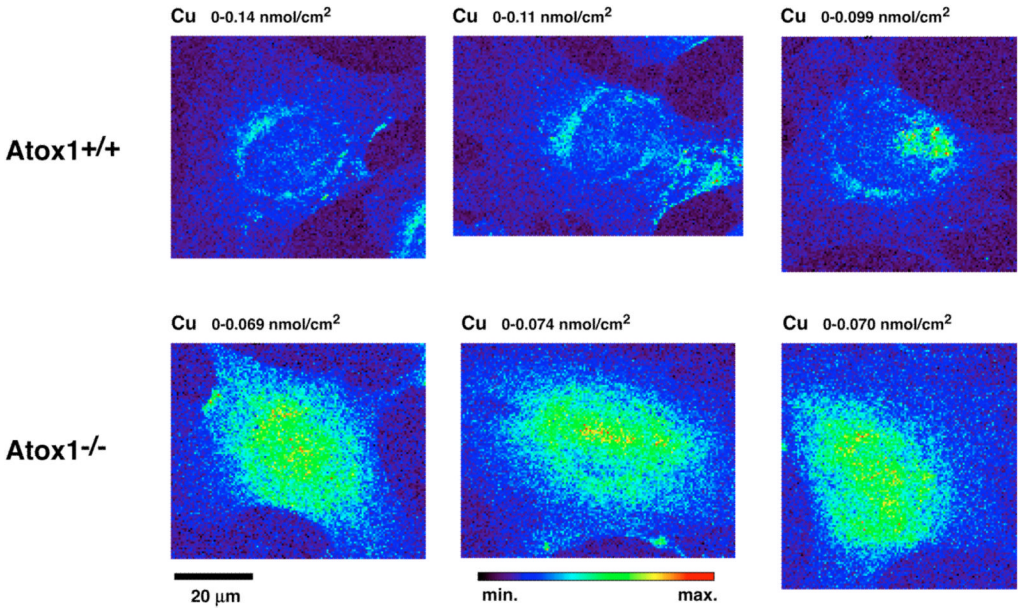

Figure 2.

False-color micrographs showing the subcellular distribution of Cu in Atox1-deficeint ($Atox1^{-/-}$) and wildtype ($Atox1^{+/+}$) cells visualized by SXRF microscopy. Cells were grown in media supplemented with 50 μM $CuCl_2$ for 4 h after pretreatment with 200 μM BCS for 48 hours. The density interval indicated above each scan refers to the full dynamic range of the false-color scale depicted in the bottom row.

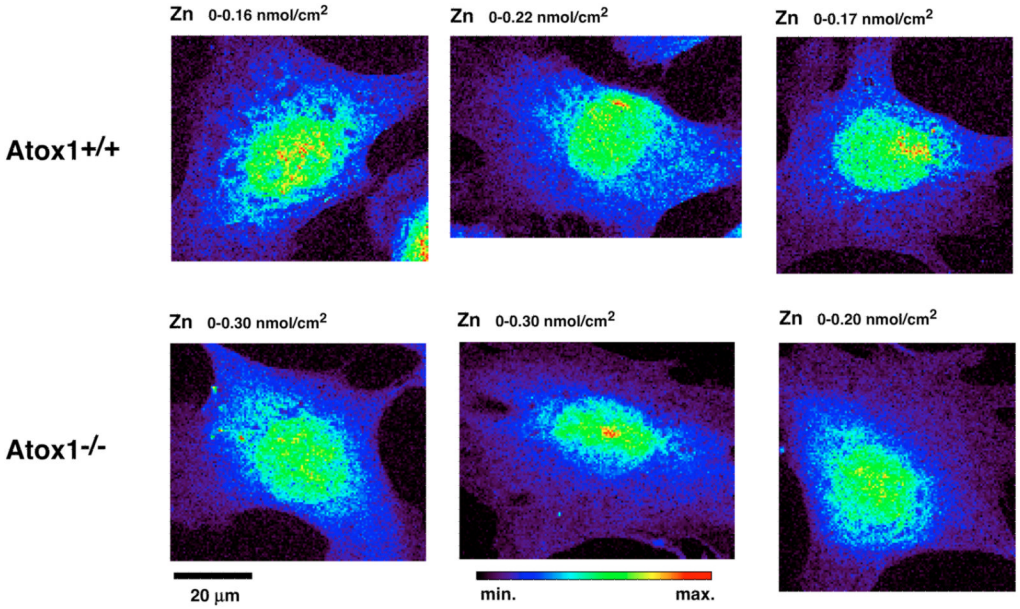

Figure 3.

False-color micrographs showing the subcellular distribution of Zn in Atox1-deficeint ($Atox1^{-/-}$) and wildtype ($Atox1^{+/+}$) cells visualized by SXRF microscopy. Cells were grown in media supplemented with 50 μM $CuCl_2$ for 4 h after pretreatment with 200 μM BCS for 48 hours. The density interval indicated above each scan refers to the full dynamic range of the false-color scale depicted in the bottom row.

Table 1

Trace metal contents of Atox1$^{+/+}$ and Atox1$^{-/-}$ cells cultured in basal medium and medium supplemented with 50 μM $CuCl_2$ for 4 h.

	basal medium [a]		50 μM $CuCl_2$/4 h [b]	
metal/ROI [c]	**Atox1$^{+/+}$**	**Atox1$^{-/-}$**	**Atox1$^{+/+}$**	**Atox1$^{-/-}$**
Cu [pmol/cm^2] [d]				
whole cell	14 ± 1	24 ± 3	25 ± 3	26 ± 2
cytoplasm	14 ± 1	22 ± 3	23 ± 4	24 ± 1
nucleus	16 ± 1	31 ± 4	31 ± 4	39 ± 1
ratio [%] [e]	23 ± 6	29 ± 3	20 ± 3	22 ± 4
Fe [pmol/cm^2] [d]				
whole cell	27 ± 1	29 ± 1	22 ± 5	27 ± 1
cytoplasm	26 ± 1	30 ± 1	22 ± 5	27 ± 1
nucleus	27 ± 1	28 ± 1	23 ± 4	29 ± 1
ratio [%][e]	20 ± 4	21 ± 6	16 ± 4	15 ± 3
Zn [pmol/cm^2] [d]				
whole cell	78 ± 10	82 ± 4	55 ± 10	67 ± 6
cytoplasm	67 ± 8	70 ± 2	46 ± 9	55 ± 5
nucleus	122 ± 4	124 ± 21	108 ± 14	134 ± 17
ratio [%][e]	33 ± 7	33 ± 7	32 ± 6	30 ± 8

[a] DMEM, 10% bovine serum, 200 mM glutamine;

[b] cells cultured basal medium and switched to medium supplemented with 50 μM $CuCl_2$ for 4 h.

[c] ROI = region of interest indicated in each row.

[d] average metal content based on three individual cells.

[e] percent ratio of the integrated nuclear metal and total cellular metal content.